

Geophysical Research Letters

RESEARCH LETTER

10.1029/2019GL082110

Key Points:

- Great heat loss and production of dense water overflow water in Nordic Seas key to the state of the MOC not the Labrador Sea
- Heat flux convergence greater than climatological estimates of subpolar gyre heat loss
- Subpolar fresh water divergence balanced by freshwater loss from Greenland shelf

Correspondence to: L. Chafik,

leon.chafik@misu.su.se

Citation

Chafik, L., & Rossby, T. (2019). Volume, heat, and freshwater divergences in the subpolar North Atlantic suggest the Nordic Seas as key to the state of the meridional overturning circulation. *Geophysical Research Letters*, 46. https://doi.org/10.1029/2019GL082110

Received 18 JAN 2019 Accepted 8 APR 2019 Accepted article online 16 APR 2019

Volume, Heat, and Freshwater Divergences in the Subpolar North Atlantic Suggest the Nordic Seas as Key to the State of the Meridional Overturning Circulation

Léon Chafik¹ and T. Rossby²

¹Department of Meteorology and Bolin Centre for Climate Research, Stockholm University, Stockholm, Sweden,

Abstract The meridional overturning circulation (MOC) decreases rapidly in subpolar and Nordic regions where the warm upper layer loses its buoyancy due to intense heat loss, sinks, and flows south. The major volume loss of the upper limb of the MOC, ~9.6 Sv out of 18.4 ± 3.4 Sv, occurs as subduction across the Iceland Basin and Irminger Sea while the major heat loss, 273 TW out of 395 ± 74 TW is associated with the MOC branch that continues into the Nordic Seas where North Atlantic deep overflow water is produced. The 122 ± 79 TW heat flux convergence in the subpolar gyre appears to be significantly larger than various estimates of heat loss to the atmosphere. Much of the 0.09 ± 0.02 Sv freshwater divergence is presumably balanced by runoff from the Greenland shelf. These estimates suggest that the Nordic Seas, not the Labrador Sea, are key to the state of the MOC.

Plain language summary The meridional overturning circulation is a two-dimensional view of the flow north of upper-ocean warm water and its return south as cold deep and intermediate water. But the actual pathways of warm-to-cold conversion are several and remarkably diverse: One branch continues into the Nordic Seas where very dense water is produced and eventually spills back into the deep North Atlantic, another branch weaves its way around the entire subpolar basin and the southern tip of Greenland to the Labrador Sea where intermediate water is formed, and the third branch is an overturning that takes place within the subpolar waters between Greenland and Scotland. Volumetrically, this is the largest branch, but in terms of heat loss the Nordic Seas, branch surrenders far more heat to the atmosphere than the other two combined. It thus plays the key role in maintaining a strong meridional overturning circulation.

1. Introduction

In recent years, the concept of a meridional overturning circulation (MOC; Buckley & Marshall, 2016) has become a widely used metric for the ocean's role in transporting heat to high latitudes in the North Atlantic. Much attention has focused on the strength of the MOC, how much water is overturned as a function of time. Significantly, most studies report an overturning transport in the 16 to 18 Sv range, a number that is largely independent of latitude (McCarthy et al., 2015 at 26°N; Willis, 2010, at 41 °N; Sarafanov et al., 2012 and Rossby et al., 2017, at 59.5 °N). But from a climate point of view it is the heat transport that is of primary interest. In contrast to volume transport, the heat transport decreases markedly as the upper limb of the MOC passes through the Gulf Stream, the North Atlantic Current and its associated branches across the subpolar North Atlantic (Figure 1). Much of the poleward decrease in heat flux reflects heat loss from within the upper limb defined by waters with density less than $\sigma_{max} = 27.55 \text{ kg/m}^3$, the density surface at which the MOC stream function reaches its maximum (Sarafanov et al., 2012) and thus does not impact the strength of the MOC. It is only when the upper limb of the MOC reaches into the subpolar North Atlantic that the accumulated heat loss densifies water to greater than σ_{max} , that is, to the lower limb, and as a consequence, the MOC decreases in strength. It is also here that the upper limb of the MOC branches form dense water in three regions: the Labrador Sea via the East Greenland Current, the subpolar basins between Greenland and Scotland, and the Nordic Seas (McCartney & Talley, 1984; Talley, 2013).

Numerous studies of volume fluxes and estimates of the MOC based on hydrographic sections across the subpolar North Atlantic have been reported (McCartney & Talley, 1984; Bacon, 1997; Sarafanov et al.,

©2019. American Geophysical Union. All Rights Reserved.

²Graduate School of Oceanography, University of Rhode Island, Kingston, RI, USA

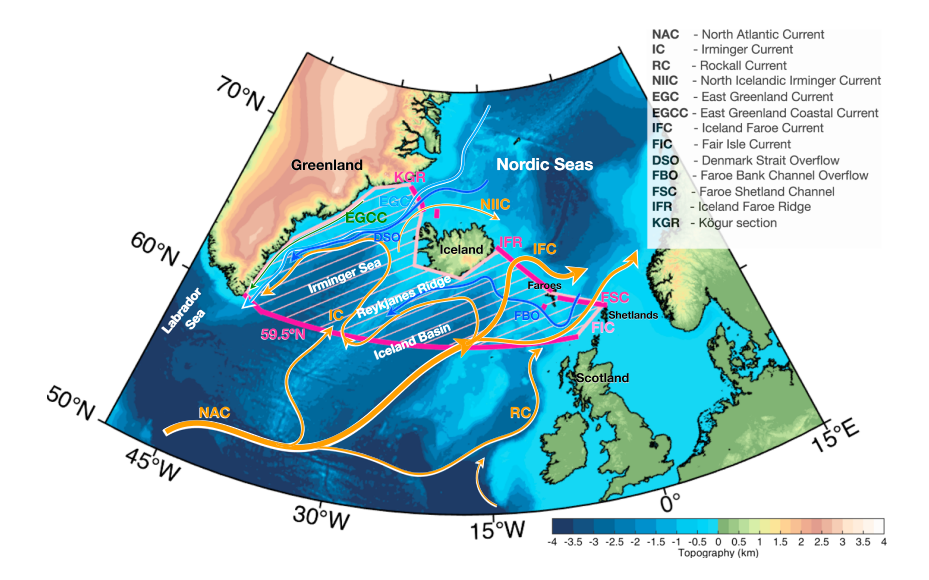


Figure 1. Bathymetric map of subpolar waters between Greenland and Scotland. It shows, in orange, the North Atlantic Current NAC with one branch, IFC, heading toward the Nordic Seas principally across the IFR and through the FSC with a contribution from the RC, and the other, which recirculates around and over the Reykjanes Ridge feeding the IC, the North Icelandic Irminger Current NICC. East of Greenland, at the shelfbreak, the south-flowing EGC is shown in light blue. The EGCC (green) hugs the coast of Greenland between the Kögur section and the southern tip of Greenland at around 59.5 °N. The deep cold FBO and DSO and their pathways are shown in dark blue. The light pink bold line and hatched area delimit the subpolar North Atlantic. All abbreviations of the currents and sections are listed in the associated panel. NAC = North Atlantic Current; IFC = Iceland-Faroe Current; IFR = Iceland-Faroe Ridge; FSC = Faroe-Shetland Channel; RC = Rockall Current; IC = Irminger Current; NIIC = North Icelandic Irminger Current; EGC = East Greenland Coastal Current; FBO = Faroe-Bank overflow; DSO = Denmark Strait overflow; KGR = Kögur section.

2012; Talley, 2013; Mercier et al., 2015; Daniault et al., 2016; Bringedal et al., 2018; Østerhus et al., 2018; Lozier et al., 2019). A few studies also address heat and fresh water fluxes (Bacon, 1997; Wijffels, 2001; Trenberth & Fasullo, 2008; Lozier et al., 2019). As technologies, measurement skills, and density of sampling improve, so have estimates of these fluxes. A significant methodological step was, for example, taken by Sarafanov et al. (2012); they used seven detailed summertime hydrographic/lowered acoustic Doppler current profiler (ADCP) sections and sea surface heights from altimetry to partition the MOC between the southern tip of Greenland and Shetland into seven subdomains to estimate flows in boundary currents and to either side of the Reykjanes Ridge.

In this study, we use two recently completed sections (Rossby et al., 2017, 2018) across the subpolar North Atlantic to quantify the branching of the upper limb and concomitant heat and freshwater divergences. The main finding is that out of the three MOC regions (subpolar gyre including Irminger Sea and Iceland Basin, the Labrador Sea, and the Nordic Seas), it is the Nordic Seas that the plays the key role. We also show that most climatologies, both reanalysis and observations only, of ocean–atmosphere heat exchange, significantly underestimate heat loss from the ocean. Last, this study estimates that the subpolar region gains fresh water from runoff from the Greenland shelf.

2. The Two MOC Sections

The two MOC sections used in this study are shown in Figure 1. The southern one (Rossby et al., 2017; hereafter called R17) uses currents measured with an ADCP on a commercial freighter, the Nuka Arctica, to construct a mean velocity field (see also Chafik et al., 2014) for the top 700 m across the subpolar North Atlantic. Hydrography from profiling Argo floats and expendable bathythermographs are used to determine the deeper ocean transports geostrophically to 1,900-m depth and World Ocean Atlas (Locarnini et al., 2013) to extend density and velocity to the bottom. The MOC strength is 18.4 ± 3.4 Sv (net volume transport; see



Table 1
The Table Is Organized By Section From Left to Right and, for Volume, Temperature and Salt Fluxes From Top to Bottom

Section	R17				R18				
Flux	EGC	59.5 °N	KGR	NIIC	IFR	FSC	FBO	FIC	SFC
Volume (Sv)									
Upper	-3.36	21.77	-0.41(-0.64)	-	3.35	3.2	-	0.3	0.019
Lower	-31.0	12.59	-5.38	0.88	1.11	-0.85	-2.2	0	-
Total	$\sum = 0 \text{ Sv}$				$\sum = 0 \text{ Sv}$				
Temperature (TW)									
Upper	-80	737	2(3)	-	109	122	-	11	-67
Lower	-500	238	-6	24	33	-20	-2	-	-
Total	$\Sigma = 395 \text{ TW}$				$\Sigma = 273 \text{ TW}$				
Salt (kg/s \times 10 ⁸)									
Upper	-1.174	7.666	-0.138(-0.216)	-	1.18	1.127	-	0.11	0.0
Lower	-10.822	4.401	-1.874	0.31	0.39	-0.3	-0.768	-	-
Total	$\Sigma = 0.071 \text{SF}$				$\Sigma = 0.037 \text{SF}$				
Freshwater (Sv)	$0.2 \pm 0.04 (loss)$				$0.11 \pm 0.01 (gain)$				0.02 (gain)

Note. The numbers for the left two columns are based on R17, and the numbers in the KGR to Faroe Bank overflow columns are based on R18. The FSC numbers are somewhat larger due to a better identification of the warm water flow there. Each cell has three rows corresponding to the upper and lower limb of the MOC defined by the $\sigma_T = 27.55 \text{ kg/m}^3$ density surface (cf. Figure 2) as well the sum of the fluxes. A minus sign always means a flow south through the section. The abbreviation SF stands for salt flux (units kg s⁻¹ × 10⁸). Gain means flux into control volume, and loss means out of control volume.

Table 1), and the corresponding heat and freshwater fluxes are 395 ± 74 TW and -0.2 ± 0.04 Sv (minus sign indicates southward flow). The two panels in Figure 2 show the mean top-to-bottom temperature and salinity fields. The solid line shows the $\sigma_{max} = 27.55$ kg/m³ shoaling nearly 1,000 m from east to west.

The northern section in Figure 1, which spans the Greenland-Scotland Ridge, is a composite of direct measurement of currents from a ferry in weekly traffic and a set of moored current meters (Rossby et al., 2018; hereafter R18). An ADCP mounted on the high-seas ferry Norröna measures currents during its transits across the Faroe-Shetland Channel (FSC) and along the Iceland-Faroe Ridge. Extending northwest from Kögur, Iceland, toward Greenland a section (hereafter KGR) comprising an array of 12 tall moorings equipped with ADCPs, and temperature and salinity recorders measure velocity and water properties across the Blosseville Basin between Iceland and the Greenland shelf (Harden et al., 2016). The volume, heat, and fresh water fluxes to the Nordic Seas according to R18 are 7.7 ± 0.8 Sv, 264 ± 27 TW, and -0.104 ± 0.01 Sv, respectively. These two Shetland/Orkney to Greenland sections encompass a 1.2×10^6 km² roughly triangular region.

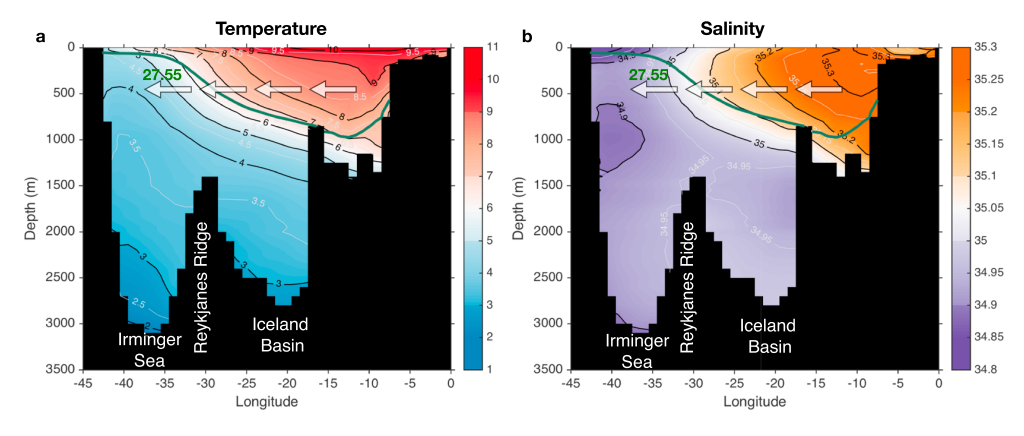


Figure 2. Ocean Atlas section of (a) temperature and (b) salinity along 59.5 °N (cf. Figure 1) between Orkney and Cape Farewell from the World Ocean Atlas 2018. The heavy green line shows the depth of the $\sigma_{max} = 27.55$ kg/m 3 isopycnal surface. The arrows indicate the cyclonic east-to-west (or warm-to-cold) movement of water across the subpolar North Atlantic.



The R17 and R18 studies of the MOC bracket a signification fraction of the North Atlantic subpolar ocean across which much of the MOC is lost from the upper limb due to heat loss to the atmosphere and resultant densification of those waters. We focus on 2012–2016 the period covered by R17. Although the R18 estimates span a longer period, 2009–2016, examination of sea-surface height gradients from altimetry (Pujol et al. 2016) shows no meaningful trend over this period so we use the 2011–2012 KGR data without any adjustment. At the most, any adjustment would be a small correction to a lesser part of the total budget. The approach will be to construct a budget of water, heat, and salt flowing through a control volume defined by the R17 and R18 sections, the surface, the bottom, Greenland in the west, and the opening between Shetland and Orkney in the east.

3. Constructing the Flux Table

A flux budget spells out all inflows and outflows, which in a steady state system should balance. From the perspective of the MOC's role in climate, the question will be to determine where and how much heat is lost to the atmosphere as the water cools, densifies, and leaves the upper limb of the MOC. The volume, temperature, and salt fluxes in and out of our control volume, that is, the subpolar North Atlantic, are given in Table 1.

3.1. The 59.5 °N Section

We separate out the East Greenland Coastal (EGC) but not the full East Greenland Coastal Current due to lack of coverage, from the net MOC to identify the principal inflow of warm, salty water into the subpolar North Atlantic north of 59.5 °N. Thus, the original 18.4 ± 3.4 Sv comprises a warm flow north of 21.77 Sv and an EGC flow south of -3.36 ± 0.12 Sv in the upper layer. Table 1 shows the corresponding temperature and salt fluxes. The lower-layer fluxes comprise the integrals of velocity and the product of velocity with temperature and salinity across all water denser than 27.55 kg/m^3 . These were determined in the R17 paper.

3.2. The Greenland-Scotland Ridge Section

The KGR section supplies cold fresh water to the control volume. The top-to-bottom transports according to the KGR array are 6.02 Sv, 3 TW, and 2.09×10^8 kg/s to the south. The entries in Table 1 show the fractions for densities less than and greater than 27.55 kg/m³. The upper layer numbers (-0.64, 3, and -0.216) are shown in a smaller font for they will be adjusted shortly. The 0.88 Sv flow north in the NIIC column in Table 1 (and corresponding entries for temperature and salt flux) refers to the North Icelandic Irminger Current. The Iceland-Faroe Ridge entry separates out the 1.11 Sv that has already been densified to >27.55 kg/m³ (estimated here from R18 data). The FSC entry shows 3.2 Sv flowing north and -0.85 Sv (flowing south) between 27.55 and 27.8 kg/m³ (estimated here from R18 data). These two add up to the 2.35 Sv flowing north for $\sigma_T < 27.8$ kg/m³ (estimated here from R18. The Faroe Bank overflow column in Table 1 accounts for $\sigma_T > 27.8$ kg/m³ (Hansen et al., 2016). Segtnan et al. (2011) obtain very similar volume and temperature transport numbers for the relevant openings defined in Rossby et al. (2018).

3.3. The Fair Isle Current (FIC)

The average flow through the opening between the Shetland and Orkney islands is about 0.3 Sv toward the North Sea (Huthnance et al., 2009; Sheehan et al., 2017; Turrell et al., 1990). Temperature and salt fluxes will be approximated by this average flow times a mean temperature and salinity of 9 °C and 35.15 respectively. This section is included for completeness, but the overall conclusions of the study would not change if the FIC were set to 0.

3.4. The East Greenland Coast

This 1,200-km long western boundary to our control volume is the one we have very little knowledge of. The flow south along this boundary consists of two parts, the East Greenland Coastal Current on the shelf (Bacon et al., 2014) and the EGC (de Steur et al., 2017), which spans the continental slope from the shelf break out. The existence of a strong salinity gradient across the system suggests that the continental slope is imposing a dynamical constraint restricting cross-frontal exchange. Some exchange must however take place, very likely by small-scale eddy processes, but how much is unclear so we assume no exchange for now.



3.5. The Surface

The 1.2 million square kilometer enclosed area is subject to summertime heating and substantial cooling in winter such that the annual average heat loss \sim 67 TW according to an ensemble of products (Figure 3); we will return to this in more detail in the next section. Evaporation (E) minus precipitation (P) is weakest in spring and greatest in fall. P-E = 0.019 Sv (P > E) into the ocean and is also discussed below.

4. Volume, Heat, and Freshwater Budgets

4.1. Volume Budget

The 2012–2016 averaging period (to filter out high-frequency variability) is thought to capture the state of a slowly varying MOC such that over this period of time it is in a near-steady state condition. Under these conditions, the two black boxes in the volume row should sum to zero since the MOC flow north should balance the flow south for each of the two sections. This adjustment can be done in many ways; we choose to follow the earlier studies (R17; R18) and do so at the Greenland end. This is readily done by reducing the flow south in the KGR column in Table 1 a small amount from -0.64 to -0.41 Sv such that flow north and south match at 8.84 Sv. This 8.84 Sv is larger than the R18 estimate due to the way flow is estimated in the FSC and the inclusion of the FIC (Østerhus et al., 2018). Given the 18.4 Sv for the southern section we infer that 9.57 Sv (18.4–8.84 Sv) is lost from the upper limb of the MOC between the two key sections. Its ± 3.5 Sv uncertainty is governed by R17 as its ± 3.4 Sv far dominates ± 0.8 Sv in R18. Of the 9.57 Sv lost through the $\sigma_t = 27.55$ kg/m³ surface, 1.99 Sv (0.88 + 1.11 Sv) continues toward the Nordic Seas as part of the overturning in the Nordic Seas while the remainder, 7.57 Sv remains in the subpolar gyre between the two sections to eventually flow back south.

4.2. Heat Budget

The condition for estimating the heat flux across the sections is that the volume fluxes balance. Having made this small flux adjustment in KGR (from -0.64 to -0.41 Sv), we obtain 273 ± 27 TW as an estimate of mean heat flux toward the Nordic Seas. This differs slightly from R18 due to the addition of the FIC. The heat flux convergence between the two lines = $395-273 = 122 \pm 79$ TW must be lost to the atmosphere assuming steady state conditions. How does this compare with estimates of climatological surface heat loss in the subpolar North Atlantic?

Figure 3 shows the annually averaged surface heat loss for the control volume (cf. Figure 1) for six surface analysis products. The top three fields (Figures 3a–3c) come from various meteorological reanalysis products (Dee et al., 2011; Kalnay et al., 1996; Kobayashi et al., 2015), while the middle three fields (Figures 3d–3f) come from various observational and satellite products (Tomita et al., 2018; Yu and Weller, 2007; Josey et al., 1999; Berry & Kent, 2011). There is a large scatter between these products ranging from 58 to 81 TW average heat loss, and the ensemble mean is ~67 TW when considering the 1988–2009 period common to all products (Figure 3g). There is also a wide range of heat loss patterns, but some common traits can be distinguished: Reanalysis products have the largest heat loss in the central subpolar North Atlantic while the objectively analyzed and satellite-derived estimates have their maximum heat loss along the EGC; this explains why the inter-product standard deviation is highest there (Figure 3h; cf. Josey et al. (2019) regarding extreme variability of heat loss in the Irminger Sea). This seems to be case even when considering a different time period and an ensemble of several other heat flux products (Yu, 2019).

It is, however, important to note that all the individual products as well as the ensemble mean heat loss estimate sum to a rate noticeably less than our ocean heat transport divergence estimate. This begs the question whether our 122 TW estimate with its 79 TW uncertainty, is helpful. For the following reasons, we find it difficult to reduce our heat loss more than 50 TW to match the above mean of the reanalysis products. First, this would require reducing the MOC by from 18.4 to \sim 14.7 Sv, that is, by almost \sim 20% or \sim 3.7 Sv (79/395*18.4 = 3.68 Sv). This is substantially below all other estimates, including especially that of Sarafanov et al. (2012). Second, although Sarafanov et al. (2012) did not report heat or fresh water fluxes, we can estimate these by multiplying the transport in each of their cells with the corresponding velocity-averaged temperature from R17; doing so, we obtain 405 TW. This large heat flux despite their lower transport (16.5 \pm 2.2 Sv) reflects a slightly different volume flux distribution, that is, they have a comparably large heat transport. Interestingly, a detailed altimetric comparison of the Sarafanov et al. (2012) observing period

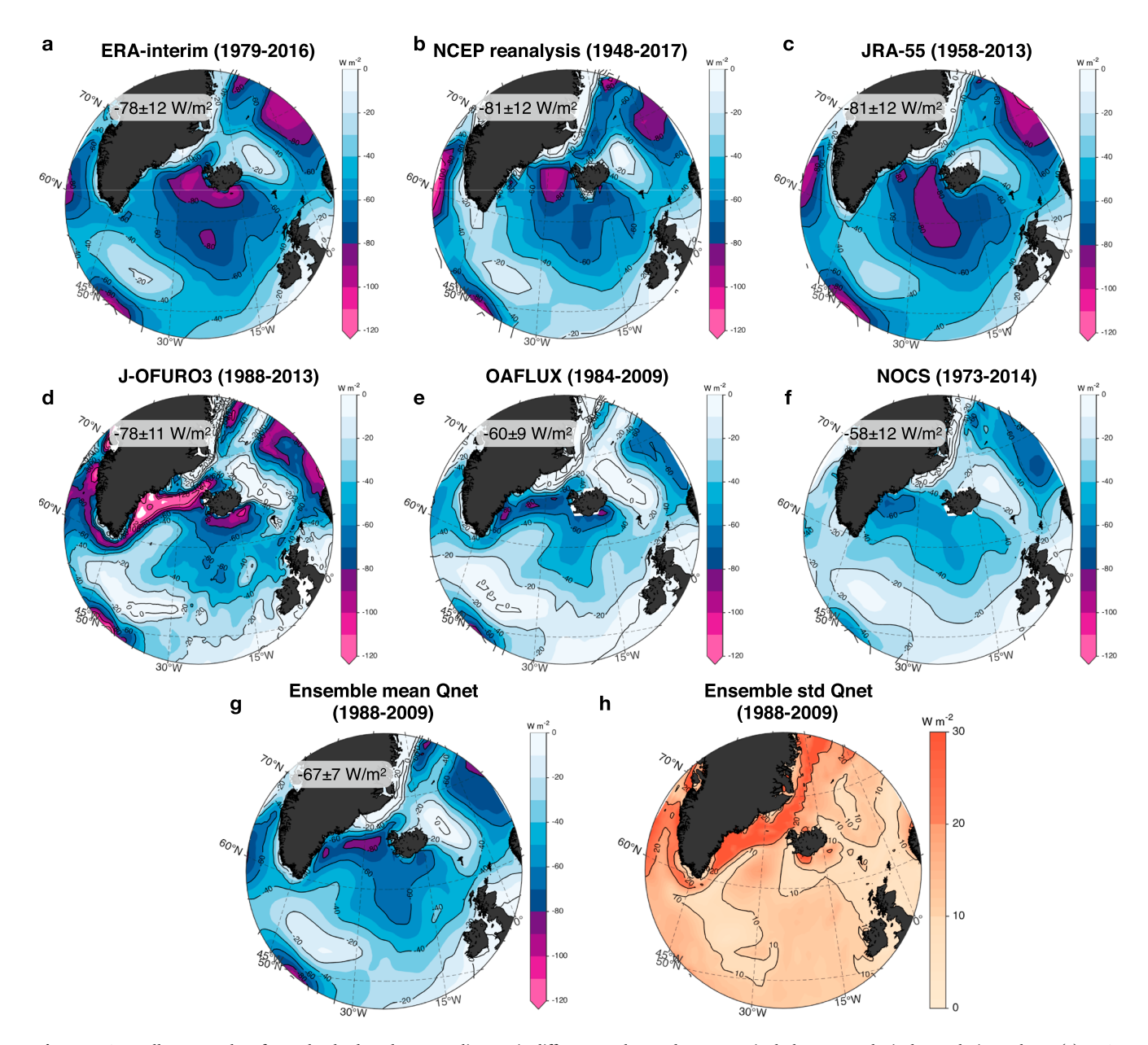


Figure 3. Annually averaged surface subpolar heat loss according to six different products. The top row includes meteorological reanalysis products, (a) ERA-Interim, (b) NCEP, and (c) JRA55. The middle row includes observational estimates consisting of (c) J-OFURO3 (satellite only), (b) OAFLUX (a blend of satellite-derived fluxes and reanalyses), and (c) NOCS (in situ) products. (g) The ensemble mean of all these products for the overlapping 1988–2009 period and (h) the associated ensemble-standard deviation. Before the ensemble averaging and standard deviation, the products were remapped onto a $0.5^{\circ} \times 0.5^{\circ}$ grid using bilinear interpolation. The numbers within each panel are the area-integrated heat fluxes (within the hatched region, cf. Figure 1) and their associated yearly mean variability for the corresponding time period.

with R17 shows no difference in mean Sea Surface Height (SSH) difference along the section (0.267 m vs. 0.270 m), but the scatter in SSH (Δ SSH) agree well with the observed scatter in transport. Thus, for the Sarafanov et al. (2012) period their fractional scatter in SSH: 0.032 m/0.267 m and transport: 2.2 Sv/16.5 Sv both equal about 0.12 while for R17 the SSH and transport ratios 0.046 m/0.270 m and 3.4 Sv/18.4 Sv both equal about 0.18. Thus, there is an internal consistency between SSH and transport variability for the two studies but not between them indicating an inherent uncertainty that can only be



reduced through additional averaging. An alternative explanation might be that the latter observing period was more variable. Giving these two studies a decade apart equal weight, we might suggest 17.4 ± 2.9 Sv and 400 ± 67 TW as a best decade-long estimate of the MOC and corresponding heat transport at 59.5 °N. The resulting heat flux convergence would be 127 ± 51 TW ($400 \pm 67-273 \pm 27$ TW). But whether or not these studies are combined, it appears that all reanalysis, objectively analyzed and satellite-based products, underestimate the heat loss to the atmosphere in the subpolar North Atlantic.

4.3. Freshwater Budget

The fresh water budget follows directly from the fresh water fluxes across R17 and R18, both of which were estimated subject to the constraint that the flux of salt north and south across each line must balance. The advantage of this method is that there is no need for a reference salinity. However, due to the slight adjustments made here to the northern section here since its publication in R18, we reestimate the fresh water flux to be -0.11 Sv (to the south into the control volume) instead of -0.104 ± 0.01 Sv, that is, virtually the same.

The difference in fresh water flux between the two lines: -0.20 ± 0.04 (out the southern line, R17) + 0.11 \pm 0.01 (in across the northern line, R18) = -0.09 ± 0.05 Sv. This fresh water loss from the enclosed volume is significantly different from zero. Precipitation minus evaporation, retrieved from ERA-interim (Dee et al., 2011), adds about 0.02 Sv (accuracy unknown). The remaining imbalance, which appears to be significant, requires an additional input of \sim 0.070 \pm 0.05 Sv. The only source we can think of is fresh water runoff from the Greenland shelf. There is, however, no clear-cut observational support for this. de Steur et al. (2017) report 70% of 65 ± 11 mSv flow at the shelfbreak with the EGC at 68 °N (referenced to 34.8), but they do not report on sea-ice transport. Bacon et al. (2014) estimate 0.07-0.08 Sv mean freshwater flux (including sea-ice transport) at 63 °N (also referenced to 34.8). Recently, Le Bras et al. (2018) report 77 mSv at Cape Farewell (referenced to 34.9). The similarity of these fluxes might suggest little fresh water loss from the Greenland shelf. This is somewhat unexpected given that Dodd et al. (2009) estimate that 49 mSv of sea ice and 15 mSv of liquid freshwater transport (referenced to 34.8) are diverted into the Nordic Seas between Fram and Denmark Straits, a distance comparable to that considered here. Furthermore, it should be noted that the Greenland ice mass comes right to the coast all along the Irminger Sea suggesting considerable precipitation and meltwater runoff from the Greenland ice sheet (Bamber et al., 2018). We also note that the Greenland shelf becomes quite narrow at 63.5 °N; could this be a place where freshwater leaves the shelf? Clearly, these are questions that need much further study not least since the interproduct standard deviation of precipitation minus evaporation are large exactly along the eastern Greenland shelf between Iceland and Cape Farewell (Yu, 2019).

Analogous to estimating heat flux in the Sarafanov et al. (2012) their fresh water flux can be estimated by multiplying transport in each of their cells with our velocity-averaged salinity and adjusting transport so there is no net salt flux. This results in a fresh water flux of -0.023 Sv. Combining this with the R17 estimate yields -0.021 Sv freshwater flux across 59.5 °N as a best estimate. This would increase the expected flux from the Greenland shelf slightly.

5. Parsing Out the Overturning

The three principal MOC overturning regions are the Labrador Sea, the subpolar region between these two sections, and the Nordic Seas. Virtually all (warm) salty water used to promote convection in the Labrador Sea must come via the EGC since very little if any comes directly from the Northwest Corner region of the North Atlantic Current (Rossby, 1996). Hence 3.36 Sv (R17) gives us a plausible estimate for the Labrador component of the MOC overturning stream function. Since the cooled water leaving the Labrador Sea can at most be cooled to 3 °C, that is, the lowest observed temperature of the convectively cooled Labrador Sea Water (Yashayaev & Loder, 2017; their Figure 2), this indicates that the corresponding heat loss can be estimated from the temperature flux into and out of the Labrador Sea: 80 TW (EGC, see R17) – 40 TW (3 °C × 4 × 10⁶ J m⁻³ °C⁻¹ heat capacity × 3.36 × 10⁶ m³/s volume transport) = 40 TW. Although their method of estimation differs, Pickart and Spall (2007) obtain a similar heat loss and suggest that the MOC is not significantly impacted by deep convection in the Labrador Sea. The subpolar basin loses 21.77 (inflow) – 3.36 (EGC) – 8.84 (Nordic Seas) = 9.57 Sv to the lower layer. The net heat lost to the Nordic Seas by that branch of the MOC is 273 ± 27 TW so the heat loss to the atmosphere = 122 ± 79 TW. It is instructive to express the estimated losses in terms of the corresponding transport. Thus, the Labrador Sea

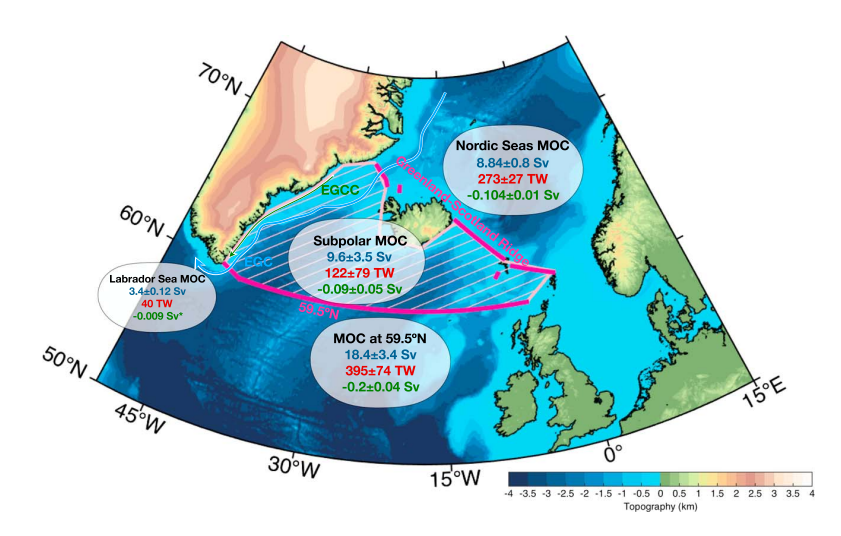


Figure 4. Schematic summary of the estimated volume (blue), heat (red), and freshwater fluxes (green) through the subpolar North Atlantic toward the Labrador Sea and Nordic Seas across the Greenland-Scotland Ridge. The star indicates that this freshwater flux is a rough estimate of what is needed to match the salt flux out of the Labrador Sea to what is supplied by the EGC (Table 3 in R17). EGC = East Greenland Current; EGCC = East Greenland Coastal Current; MOC = meridional overturning circulation.

loses 11.9 TW/Sv (40/3.36 TW/Sv), the subpolar region 12.7 TW/Sv (122/9.57 TW/Sv), and the Nordic Seas 30.9 TW/Sv (273/8.84 TW/Sv). The significantly greater loss rate for the Nordic Seas is another way of noting that the temperature difference between the water flowing north and the water spilling back into the North Atlantic is much greater than for either the Labrador Sea or subpolar gyre. It should also be noted that Østerhus et al. (2018; their Table 2) report no long-term trends of the observed exchanges across the Greenland-Scotland Ridge. Figure 4 summarizes the partitioning of the MOC fluxes between the Labrador Sea, the subpolar gyre, and the Nordic Seas. A recent publication by Lozier et al. (2019) concludes that Labrador Sea is not a key player in the conversion of light-to-dense water in the MOC. We agree with their results and would take this a step further and point to the key role of the Nordic Seas for the MOC stability. It is the overflow of dense water and its entrainment of intermediate density water in the Subpolar North Atlantic that sustain the lower limb of the MOC.

Interestingly, the MOC overturning in the subpolar region can be viewed as a form of lateral subduction. As the east flowing North Atlantic current water wends its way from east to west curving around or crossing over the Reykjanes Ridge (Childers et al., 2015; Petit et al., 2018), it is cooled every winter to a progressively greater density. As a result, the average depth of the 27.55 kg/m³ isopycnal shoals from about 1,000-m depth in the east to where it is almost vanishes at 50 m in the west (at 59.5 °N; R17). Thus, as a fluid parcel traverses this space, it will move from the upper layer of the MOC into the lower layer in a strongly time-dependent process, moving into the lower layer and back out between winter and summer (e.g., Lazarevich et al., 2004) but remaining in the lower layer longer for each passing winter until it is permanently subducted (Cushman-Roisin, 1987). It is the shoaling of the interface from east to west, cf. Figure 2, rather than a descent or sinking of water that defines the "overturning" of the MOC here.

6. Summary

Thanks to two commercial vessels in regular traffic, two highly resolved sections of currents in the subpolar North Atlantic enable us to construct an estimate of where the upper limb of the MOC overturns and the associated heat losses. Of the 21.77 Sv warm water flow crossing 59.5 °N, 3.36 ± 0.12 Sv flows south in the EGC rounding the southern tip of Greenland toward the Labrador Sea. The 8.84 ± 0.8 Sv volume transport into the Nordic Seas is slightly larger than past estimates because it identifies more clearly the transport north in the Faroe-Shetland Channel and also includes 0.3 Sv in the Faroe-Isle Current. The remaining volume flow, that is, 9.6 Sv, leaves the upper limb of the MOC in the subpolar gyre between the two



sections through convectively driven lateral subduction. The much larger heat losses in the Nordic Seas, 273 ± 27 TW, than the sum of both the Labrador Sea (40 TW) and subpolar waters (122 TW), reinforces the view that strength of the MOC is largely governed by the production of dense water north of the Greenland-Scotland Ridge. The large freshwater convergence can plausibly be accounted for by a freshwater leakage from the East Greenland shelf, but this needs much more study. Lastly, we find that our estimated ocean heat flux convergence in the subpolar North Atlantic appears to be significantly greater than available heat flux products, whether produced by meteorological reanalyses, ocean observations, or satellite derived. The principal source of uncertainty in this study comes from limited number of vessel-transects sampling oceanic variability along the southern section (R17). Nonetheless, these results point to the power and cost effectiveness of repeat profiling of currents and temperature along select vessel routes and combining these data with altimetry and Argo profiles to determine the strength of the MOC and concomitant heat and fresh water fluxes.

Acknowledgments

L. C. acknowledges support through the Swedish National Space Agency (Dnr 133/17) and the FiNNESS project. The data sets used in this study were first published in R17 and R18 and are publically available via http://po.msrc. sunvsb.edu/Norrona/ and by contacting Dr. Henrik Søiland (henrik. soiland@imr.no) at the Institute of Marine Research, Bergen, Norway. The air-sea flux data was obtained through the research data archive (https://rda. ucar.edu). The J-OFURO3 air-sea flux data was obtained through the website (https://j-ofuro.scc.u-tokai.ac.jp/en/). T. R. would like to thank the International Meteorological Institute at the University of Stockholm for its hospitality where much of this work was done. We thank the two reviewers for many helpful suggestions for improving the presentation of this

References

- Bacon, S. (1997). Circulation and fluxes in the North Atlantic between Greenland and Ireland. *Journal of Physical Oceanography*, 27(7), 1420–1435. https://doi.org/10.1175/1520-0485(1997)027<1420:CAFITN>2.0.CO:2
- Bacon, S., Marshall, A., Holliday, N. P., Aksenov, Y., & Dye, S. R. (2014). Seasonal variability of the East Greenland coastal current. *Journal of Geophysical Research: Oceans*, 119, 3967–3987. https://doi.org/10.1002/2013JC009279
- Bamber, J. L., Tedstone, A. J., King, M. D., Howat, I. M., Enderlin, E. M., van den Broeke, M. R., & Noel, B. (2018). Land ice freshwater budget of the Arctic and North Atlantic oceans: 1. Data, methods, and results. *Journal of Geophysical Research: Oceans*, 123, 1827–1837. https://doi.org/10.1002/2017JC013605
- Berry, D. I., & Kent, E. C. (2011). Air–Sea fluxes from ICOADS: The construction of a new gridded dataset with uncertainty estimates. International Journal of Climatology, 31(7), 987–1001. https://doi.org/10.1002/joc.2059
- Bringedal, C., Eldevik, T., Skagseth, Ö., Spall, M. A., & Østerhus, S. (2018). Structure and forcing of observed exchanges across the Greenland-Scotland ridge. *Journal of Climate*, 31(24), 9881–9901. https://doi.org/10.1175/JCLI-D-17-0889.1
- Buckley, M. W., & Marshall, J. (2016). Observations, inferences, and mechanisms of Atlantic meridional overturning circulation variability: A review. Reviews of Geophysics, 54, 5–63. https://doi.org/10.1002/2015RG000493
- Chafik, L., Rossby, T., & Schrum, C. (2014). On the spatial structure and temporal variability of poleward transport between Scotland and Greenland. *Journal of Geophysical Research: Oceans, 119*, 824–841. https://doi.org/10.1002/2013JC009287
- Childers, K. H., Flagg, C. N., Rossby, T., & Schrum, C. (2015). Directly measured currents and estimated transport pathways of Atlantic water between 59.5 °N and the Iceland-Faroes-Scotland ridge. *Tellus A*, 67(1), 28067. https://doi.org/10.3402/tellusa.v67.
- Cushman-Roisin, B. (1987). Subduction. In P. Müller & D. Henderson (Eds.), 'Dynamics of the oceanic surface mixed-layer'. Aha-Hulikoa Series (pp. 181–196). Honolulu: Hawaiian Institute of Geophysics.
- Dee, D. P., Uppala, S. M., Simmons, A. J., Berrisford, P., Poli, P., Kobayashi, S., et al. (2011). The ERA-interim reanalysis: Configuration and performance of the data assimilation system. *Quarterly Journal of the Royal Meteorological Society*, 137(656), 553–597. https://doi.org/10.1002/qi.828
- de Steur, L., Pickart, R. S., Macrander, A., Våge, K., Harden, B., Jonsson, S., et al. (2017). Liquid freshwater transport estimates from the East Greenland current based on continuous measurements north of Denmark Strait. *Journal of Geophysical Research: Oceans*, 122, 93–109. https://doi.org/10.1002/2016JC012106
- Dodd, P. A., Heywood, K. J., Meredith, M. P., Naveira-Garabato, A. C., Marca, A. D., & Falkner, K. K. (2009). Sources and fate of freshwater exported in the East Greenland current. *Geophysical Research Letters*, 36, L19608. https://doi.org/10.1029/2009GL039663
- Hansen, B., Larsen, K. M. H., Hátún, H., & Østerhus, S. (2016). A stable Faroe Bank Channel overflow 1995–2015. Ocean Science, 12(6), 1205–1220. https://doi.org/10.5194/os-12-1205-2016
- Harden, B. E., Pickart, R. S., Valdimarsson, H., Våge, K., de Steur, L., Richards, C., et al. (2016). Upstream sources of the Denmark Strait overflow: Observations from a high-resolution mooring array. Deep Sea Research Part I: Oceanographic Research Papers, 112, 94–112. https://doi.org/10.1016/j.dsr.2016.02.007
- Huthnance, J. M., Holt, J. T., & Wakelin, S. L. (2009). Deep ocean exchange with west-European shelf seas. Ocean Science, 5(4), 621–634. www.ocean-sci.net/5/621/2009/, https://doi.org/10.5194/os-5-621-2009
- Josey, S. A., de Jong, M. F., Oltmanns, M., Moore, G. K., & Weller, R. A. (2019). Extreme variability in Irminger Sea winter heat loss revealed by ocean observatories initiative mooring and the ERA5 reanalysis. *Geophysical Research Letters*, 46, 293–302. https://doi.org/10.1029/2018GL080956
- Josey, S. A., Kent, E. C., & Taylor, P. K. (1999). New insights into the ocean heat budget closure problem from analysis of the SOC air-sea flux climatology. *Journal of Climate*, 12(9), 2856–2880. https://doi.org/10.1175/1520-0442(1999)012<2856:NIITOH>2.0.CO;2
- Kalnay, E., Kanamitsu, M., Kistler, R., Collins, W., Deaven, D., Gandin, L., et al. (1996). The NCEP/NCAR 40-year reanalysis project. Bulletin of the American Meteorological Society, 77(3), 437–471. https://doi.org/10.1175/1520-0477(1996)077<0437:TNYRP>2.0.CO;2
- Kobayashi, S., Ota, Y., Harada, Y., Ebita, A., Moriya, M., Onoda, H., et al. (2015). The JRA-55 reanalysis: General specifications and basic characteristics. Journal of the Meteorological Society of Japan. Ser. II, 93(1), 5–48. https://doi.org/10.2151/jmsj.2015-001
- Lazarevich, P., Rossby, T., & McNeil, C. (2004). Oxygen variability in the near-surface waters of the northern North Atlantic: Observations and a model. *Journal of Marine Research*, 62(5), 663–683. https://doi.org/10.1357/0022240042387547
- Le Bras, I. A.-A., Straneo, F., Holte, J., & Holliday, N. P. (2018). Seasonality of freshwater in the East Greenland current system from 2014 to 2016. *Journal of Geophysical Research: Oceans*, 123, 8828–8848. https://doi.org/10.1029/2018JC014511
- Locarnini, R. A., Mishonov, A. V., Antonov, J. I., Boyer, T. P., Garcia, H. E., Baranova, O. K., et al. (2013). In S. Levitus, & A. Mishonov (Eds.), World Ocean Atlas 2013, Volume 1: Temperature, NOAA Atlas NESDIS (Vol. 73, p. 40).
- Lozier, M. S., Li, F., Bacon, S., Bahr, F., Bower, A. S., Cunningham, S. A., et al. (2019). A sea change in our view of overturning in the subpolar North Atlantic. Science, 363(6426), 516–521. https://doi.org/10.1126/science.aau6592



- McCarthy, G. D., Smeed, D. A., Johns, W. E., Frajka-Williams, E., Moat, B. I., Rayner, D., et al. (2015). Measuring the Atlantic meridional overturning circulation at 26 °N. Progress in Oceanography, 130, 91–111. https://doi.org/10.1016/j.pocean.2014.10.006
- McCartney, M. S., & Talley, L. D. (1984). Warm-to-cold water conversion in the northern North Atlantic Ocean. *Journal of Physical Oceanography*, 14(5), 922–935. https://doi.org/10.1175/1520-0485(1984)014<0922:WTCWCI>2.0.CO;2
- Mercier, H., Lherminier, P., Sarafanov, A., Gaillard, F., Daniault, N., Desbruyères, D., et al. (2015). Variability of the meridional over-turning circulation at the Greenland-Portugal OVIDE section from 1993 to 2010. *Progress in Oceanography*, 132, 250–261. https://doi.org/10.1016/j.pocean.2013.11.001
- Østerhus, S., Woodgate, R., Valdimarsson, H., Turrell, B., de Steur, L., Quadfasel, D., et al. (2018). Arctic Mediterranean exchanges: A consistent volume budget and trends in transports from two decades of observations. Ocean Science Discussions, 1–37. https://doi.org/10.5194/os-2018-114
- Pujol, M. I., Fauge're, Y., Taburet, G., Dupuy, S., Pelloquin, C., Ablain, M., & Picot, N. (2016). DUACS DT2014: The new multi-mission altimeter data set reprocessed over 20 years. Ocean Science, 12(5), 1067–1090. https://doi.org/10.5194/os-12-1067-2016
- Petit, T., Mercier, H., & Thierry, V. (2018). First direct estimates of volume and water mass transports across the Reykjanes ridge. *Journal of Geophysical Research: Oceans*, 123, 6703–6719. https://doi.org/10.1029/2018JC013999
- Pickart, R. S., & Spall, M. A. (2007). Impact of Labrador Sea convection on the North Atlantic meridional overturning circulation. *Journal of Physical Oceanography*, 37(9), 2207–2227. https://doi.org/10.1175/JPO3178.1
- Rossby, T. (1996). The North Atlantic current and surrounding waters: At the crossroads. Reviews of Geophysics, 34(4), 463–481. https://doi.org/10.1029/96RG02214
- Rossby, T., Flagg, C., Chafik, L., Harden, B., & Søiland, H. (2018). A direct estimate of volume, heat and fresh water exchange across the Greenland-Iceland-Faroe-Scotland ridge. *Journal of Geophysical Research: Oceans*, 123, 7139–7153. https://doi.org/10.1029/ 2018JC014250
- Rossby, T., Reverdin, G., Chafik, L., & Søiland, H. (2017). A direct estimate of poleward volume, heat, and freshwater fluxes at 59.5 °N between Greenland and Scotland. *Journal of Geophysical Research: Oceans, 122,* 5870–5887. https://doi.org/10.1002/2017JC012835
- Sarafanov, A., Falina, A., Mercier, H., Sokov, A., Lherminier, P., Gourcuff, C., et al. (2012). Mean full-depth summer circulation and transports at the northern periphery of the Atlantic Ocean in the 2000s. *Journal of Geophysical Research*, 117, C01014. https://doi.org/ 10.1029/2011JC007572
- Segtnan, O. H., Furevik, T., & Jenkins, A. D. (2011). Heat and freshwater budgets of the Nordic Seas computed from atmospheric reanalysis and ocean observations. *Journal of Geophysical Research*, 116, C11003. https://doi.org/10.1029/2011JC006939
- Sheehan, P. M. F., Berx, B., Gallego, A., Hall, R. A., Heywood, K. J., & Hughes, S. L. (2017). Thermohaline forcing and interannual variability of northwestern inflows into the northern North Sea. Continental Shelf Research, 138, 120–131. https://doi.org/10.1016/j.csr.2017.01.016
- Talley, L. D. (2013). Shallow, intermediate, and deep overturning components of the global heat budget. *Journal of Physical Oceanography*, 33, 530–560.
- Tomita, H., Hihara, T., Kako, S., Kubota, M., & Kutsuwada, K. (2018). An introduction to J-OFURO3, A third-generation Japanese ocean flux data set using remote-sensing observations. *Journal of Oceanography*, 75(2), 171–194. https://doi.org/10.1007/s10872-018-0493-x
- Trenberth, K. E., & Fasullo, J. T. (2008). An observational estimate of inferred ocean energy divergence. *Journal of Physical Oceanography*, 38(5), 984–999. https://doi.org/10.1175/2007JPO3833.1
- Turrell, W. R., Henderson, E. W., & Slesser, G. (1990). Residual transport within the Fair Isle current observed during the autumn circulation experiment (ACE). Continental Shelf Research, 10(6), 521–543. https://doi.org/10.1016/0278-4343(90)90080-6
- Wijffels, S. E. (2001). Ocean transport of fresh water, in ocean circulation and climate, edited by G. Siedler, J. church, and J. Gould, chap. 6.2. International Geophysics Series, 77, 715.
- Willis, J. (2010). Can in situ floats and satellite altimeters detect long-term changes in the Atlantic Ocean overturning? Geophysical Research Letters, 37, L06602. https://doi.org/10.1029/2010GL042372
- Yashayaev, I., & Loder, J. W. (2017). Further intensification of deep convection in the Labrador Sea in 2016. Geophysical Research Letters, 44, 1429–1438. https://doi.org/10.1002/2016GL071668
- Yu, L. (2019). Global air-sea fluxes of heat, fresh water, and momentum: Energy budget closure and unanswered questions. Annual Review of Marine Science, 11(1), 227–248. https://doi.org/10.1146/annurev-marine-010816-060704
- Yu, L., & Weller, R. A. (2007). Objectively analyzed air-sea heat fluxes for the global ice-free. Oceans (1981–2005). Bulletin of the American Meteorological Society, 88(4), 527–540. https://doi.org/10.1175/BAMS-88-4-527